Latin American Journal of Solids and Structures

Prediction of Modal Damping of FRP-Honeycomb Sandwich Panels with Arbitrary Geometries

Abstract

In this work, the modal characteristics, including modal damping, of FRP composite skin, honeycomb core sandwich panels with arbitrary geometries are computed using a mixed finite element-meshless method. By using the meshless node distribution scheme in conjunction with the lagrangian quadrilateral interpolating functions, the continuity of inter-elemental displacements is assured. Since the distribution of the elements is not limited to the geometry of the problem, any arbitrary geometry can be readily analysed by using the same node and element distributions. Using the first order shear deformation plate theory, together with a structural damping model, modal response results are produced for a number of sandwich panel geometries, including triangular, trapezoidal, circular as well as rectangular plates with different combinations of free and clamped edges. Results are compared with those reported in the literature, showing the viability and the accuracy of the method.

A. Abbasloo [a]
M.R. Maheri [b]

[a] Department of Mechanical Engineering, Shahid Bahonar University of Kerman, Iran. Email: aslan.abbasloo@sirjantech.ac.ir
[b] Department of Mechanical Engineering, Shahid Bahonar University of Kerman, Iran. Email: mrmaheri@uk.ac.ir

1 INTRODUCTION

Aerospace structures bearing lateral loads are normally made from a light, spacer core sandwiched between two load-bearing skins. Increasingly, aerospace sandwich materials have fibre reinforced polymer (FRP) composites as their skins, and often a honeycomb material made from resin-soaked paper as their core. Compared to the traditional aluminium sandwich, not only do these materials enjoy a greater stiffness to weight ratio, they are also far more damped.

Sandwich modal damping is a function of several factors, including the sandwich skin/core damping and thickness ratio, its planar aspect ratio and its end conditions. With multilayer FRP

skins, the skin damping capacity will itself be a function of layer orientation and stacking sequence. (Maheri et al., 2008; Maheri and Adams, 1994; Thamburaj and Sun, 2001).

Some work on sandwich damping (Soovere, 1984; Meunier and Shenoi, 2001) have used a rate-dependent viscoelastic damping model while others (Maheri et al., 2008; Koo and Lee, 1995; Yim and Gillespie, 2000) have opted for a simpler rate-independent structural damping model. Most often, carbon and glass fibre FRP composites can be considered to be rigid enough to render the viscoelastic effect negligible. A viscoelastic analysis, however, lends itself more to situations where highly viscoelastic materials are purposely added to the structure as a constrained or free layer to increase damping.

Sandwich modal properties has long attracted a considerable attention. Various theories have been proposed regarding the mechanics of sandwich deformation and damping. Often, a simple, first order shear deformation theory has been used (Maheri et al., 2008; Liu and Zhao, 2001; Zhao and Stronge, 2006). To describe the sandwich shear deformation more accurately, higher order shear deformation theories have been developed (Liu and Zhao, 2007; Elmalichand Rabinovitch, 2012; Phan et al., 2013). Numerous factors influence sandwich damping, and these too have been the subject of some investigations (Maheri et al., 2008; Maheri and Adams, 1994; Thamburaj and Sun, 2001; Yaman and Onal, 2015).

The sandwich panels considered in the above studies have generally been of a rectangular shape. The primary aim of the present work was to devise a method through which FRP-Honeycom sandwich panels with any arbitrary geometry and boundary conditions could be readily and conveniently analysed for their modal characteristics, particularly structural damping. The first order shear deformation theory is used for sandwich deformation since any refinement in the damping results produced by a higher order theory is well within the expected tolerance of damping measurements. We have used a combination of the meshless node distribution and the finite element (FE) techniques in which, similar to the latter method, rectangular elements are arranged side by side so that they cover the domain of the problem, while the meshless technique is used to ensure the inter-elemental continuity of the displacement functions and their derivatives. The meshless node distribution wholly covers the problem domain, and the boundary elements are of the same rectangular shape as the elements that lie within the geometric domain. Since some boundary elements could extend beyond the geometric bonds of the problem, the actual boundary is defined at the integration stage where the energies are computed only within the problem domain. Because the geometric bounds of the particular problem are independent of the node and element distributions, the same predefined nodal and elemental distributions may be used to analyse any arbitrary shape, thereby saving on computational and human resources.

The proposed method in the present work has been compared with the Rayleigh-Ritz analysis of (Maheri et al., 2008). It is noted that while any arbitrarily shaped plate can be solved using the present method, the Rayleigh-Ritz analysis is limited to the solution of rectangular plates.

A number of panel geometries, including triangular, trapezoidal, circular as well as rectangular shapes have been considered. Both clamped and free edges have been considered for the sandwich boundary conditions. Where available, the results have been compared with those previously reported in the literature.

2 THEORY

The discretization scheme used in the present work is based on a combination of the finite element and the meshless methods. Considering an element of a mid-plane symmetric sandwich plate with FRP skins and a honeycomb core (Figure 1), the displacements within the element are functions of the displacements in the sixteen surrounding nodes. As in the FE scheme, the sixteen-noded lagrangian quadrilateral is duly used for interpolation. These sixteen nodes constitute part of the meshless support domain for the points inside the element.
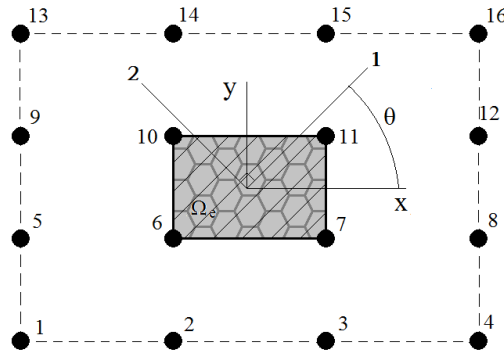
Figure 1: Sandwich panel element in a meshless node distribution.

Shown in Figure 2 is a 3-D diagram of the sandwich plate and its assumed DOFs which include the displacement w in the z-direction, and the two total rotations ψ_x and ψ_y about the y- and the x-axes respectively. Each rotation comprises the rotation due to bending and the rotation due to transverse shear.
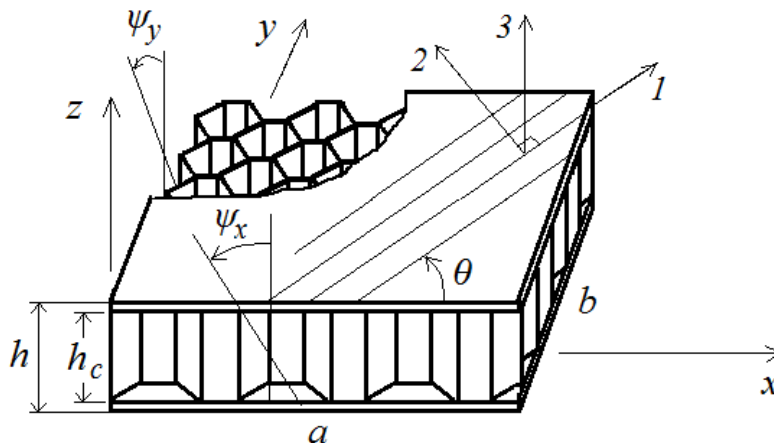

Figure 2: 3-D vision of sandwich panel and its DOFs.

The plate's displacement field according to the first order shear deformation theory is given as

$$u_x = -\psi_x\, z$$
$$u_y = -\psi_y\, z$$
$$w = w(x, y)$$

Using the following usual convention in referring to the stress and strain components,

$$\mathrm{xx} \to 1, \mathrm{yy} \to 2, \mathrm{zz} \to 3, \mathrm{xz} \to 4, \mathrm{yz} \to 5, \mathrm{xy} \to 6$$

Then strain components $\{\varepsilon\}$ are found from Equations (1) as

$$\{\varepsilon\} = \begin{Bmatrix} \varepsilon_1 \\ \varepsilon_2 \\ \varepsilon_4 \\ \varepsilon_5 \\ \varepsilon_6 \end{Bmatrix} = \begin{Bmatrix} -\dfrac{\partial \psi_x}{\partial x}\, z \\[2mm] -\dfrac{\partial \psi_y}{\partial y}\, z \\[2mm] (-\psi_x + \dfrac{\partial w}{\partial x}) \\[2mm] (-\psi_y + \dfrac{\partial w}{\partial y}) \\[2mm] -(\dfrac{\partial \psi_x}{\partial y} + \dfrac{\partial \psi_y}{\partial x})\, z \end{Bmatrix} == \begin{Bmatrix} \chi_1 z \\ \chi_2 z \\ \chi_4 \\ \chi_4 \\ \chi_6 z \end{Bmatrix} \tag{1}$$

Assuming that the strain energy of the sandwich element shown in Figure 1 is a piecewise function of the strain energies of the skins and the core, then it can be written as

$$U_e = \frac{1}{2}\sum_{k=1}^{L}\int_{z_{k-1}}^{z_k} (\int_{\Omega_e} \{\varepsilon\}^T \left[\overline{Q}^{(k)}\right]\{\varepsilon\}\, dxdy)dz + \frac{1}{2}\int_{-\frac{h_c}{2}}^{\frac{h_c}{2}} (\int_{\Omega_e} \{\varepsilon\}^T [G_c]\{\varepsilon\}\, dxdy)dz \tag{2}$$

in which L is the total number of layers in both skins, z_k and $z_{(k-1)}$ are the distances from the sandwich mid-plane to the outer and the inner faces of the kth layer of the skins respectively, h_c is the core thickness, and

$$\left[\overline{Q}\right] = [T_\sigma][Q]\left[T_\varepsilon^{-1}\right] \tag{3.1}$$

$$[G_c] = \begin{bmatrix} 0 & 0 & 0 & 0 & 0 \\ & 0 & 0 & 0 & 0 \\ & & G_{xz} & 0 & 0 \\ & Sym & & G_{yz} & 0 \\ & & & & 0 \end{bmatrix} \tag{3.2}$$

where $\left[\overline{Q}\right]$ is the off-axis, plane stress orthotropic stiffness matrix for each layer k of the FRP laminate skins, and $\left[G_c\right]$ is the stiffness matrix of the core. The off-axis stiffness matrix $\left[\overline{Q}\right]$ is given in terms of the on-axis stiffness matrix, $[Q_{ij}]$, whose components are given in terms of the orthotropic elastic property constants of the skins as

$$[Q_{ij}] = \begin{bmatrix} \dfrac{E_1^2}{E_1 - v_{12}{}^2 E_2} & \dfrac{v_{12}E_1E_2}{E_1 - v_{12}{}^2 E_2} & 0 & 0 & 0 \\[2ex] & \dfrac{E_1 E_2}{E_1 - v_{12}{}^2 E_2} & 0 & 0 & 0 \\[2ex] & & G_{12} & 0 & 0 \\[2ex] & & & \dfrac{E_2}{2(1+v_{23})} & 0 \\[2ex] \text{Sym.} & & & & G_{12} \end{bmatrix} \tag{4}$$

The stress and strain transformation matrices in equation (1) are given as

$$[T_\varepsilon] = \begin{bmatrix} m^2 & n^2 & 0 & 0 & -mn \\ n^2 & m^2 & 0 & 0 & mn \\ 0 & 0 & m & -n & 0 \\ 0 & 0 & n & m & 0 \\ 2mn & -2mn & 0 & 0 & m^2-n^2 \end{bmatrix}, \quad [T_\sigma] = \begin{bmatrix} m^2 & n^2 & 0 & 0 & -2mn \\ n^2 & m^2 & 0 & 0 & 2mn \\ 0 & 0 & m & -n & 0 \\ 0 & 0 & n & m & 0 \\ mn & -mn & 0 & 0 & m^2-n^2 \end{bmatrix} \tag{5}$$

where $m = \cos(\theta)$ and $n = \sin(\theta)$

It is noted that Equations (3) and (4) reflect the assumption that while the in-plane damping of the honeycomb material can always be neglected with little loss of accuracy, the shear damping of the skins can be significant depending on the skin/core relative thickness.

Equation (1) in equation (2) will give

$$U_e = \sum_{k=1}^{L} (\int_{\Omega_e} (k_s (\overline{Q}_{45}^{(k)} \chi_4 \chi_5 + \frac{1}{2}\overline{Q}_{44}^{(k)} \chi_4^2 + \frac{1}{2}\overline{Q}_{55}^{(k)} \chi_5^2)(z_k - z_{k-1})$$

$$+ \frac{1}{6}(\overline{Q}_{11}^{(k)}\chi_1^2 + \overline{Q}_{22}^{(k)}\chi_2^2 + \overline{Q}_{66}^{(k)}\chi_6^2 + 2\overline{Q}_{12}^{(k)}\chi_1\chi_2 + 2\overline{Q}_{16}^{(k)}\chi_1\chi_6 + 2\overline{Q}_{26}^{(k)}\chi_2\chi_6) \tag{6}$$

$$\times (z_k^3 - z_{k-1}^3)) dxdy) + \frac{1}{2}k_s h_c \int_{\Omega_e} (G_{xz}\chi_4^2 + G_{yz}\chi_5^2) dxdy$$

in which k_s is a shear correction factor, normally assumed to be about 5/6. For each node p, the displacements can be written in terms of the 16-noded lagrangian interpolating functions (ϕ_i) as

$$
\begin{aligned}
w(x,y) &= \phi_i w_i \\
\psi_x(x,y) &= \phi_i \psi_{xi} \quad , \quad i = 1,2,3\ldots16 \\
\psi_y(x,y) &= \phi_i \psi_{yi}
\end{aligned}
\tag{7}
$$

Therefore, the curvatures $\{\chi\}$ in equation (1) can be written as

$$
\begin{aligned}
\chi_1 &= -\frac{\partial \phi_i}{\partial x}\psi_{xi} \\[6pt]
\chi_2 &= -\frac{\partial \phi_i}{\partial y}\psi_{yi} \\[6pt]
\chi_4 &= -\phi_i\psi_{xi} + \frac{\partial \phi_i}{\partial x}w_i \qquad , \quad i = 1,2,3\ldots16 \\[6pt]
\chi_5 &= -\phi_i\psi_{yi} + \frac{\partial \phi_i}{\partial y}w_i \\[6pt]
\chi_6 &= -(\frac{\partial \phi_i}{\partial y}\psi_{xi} + \frac{\partial \phi_i}{\partial x}\psi_{yi})
\end{aligned}
\tag{8}
$$

Substituting equation (8) in equation (6) will give the element's strain energy as

$$
U_e = A_{ij}w_iw_j + B_{ij}w_i\psi_{xj} + C_{ij}w_i\psi_{yj} + D_{ij}\psi_{xi}\psi_{xj} + F_{ij}\psi_{yi}\psi_{yj} + H_{ij}\psi_{xi}\psi_{yj}
\tag{9}
$$

in which

$$
\begin{aligned}
A_{ij} &= \frac{1}{2}k_s h_c \int_{\Omega_e} (G_{xz}\frac{\partial \phi_i}{\partial x}\frac{\partial \phi_j}{\partial x} + G_{yz}\frac{\partial \phi_i}{\partial y}\frac{\partial \phi_j}{\partial y})\mathrm{d}x\mathrm{d}y + \frac{1}{2}k_s\sum_{k=1}^{L}(z_k - z_{k-1}) \\[6pt]
&(\int_{\Omega_e}(\overline{Q}_{44}^{(k)}\frac{\partial \phi_i}{\partial x}\frac{\partial \phi_j}{\partial x} + \overline{Q}_{55}^{(k)}\frac{\partial \phi_i}{\partial y}\frac{\partial \phi_j}{\partial y} + \overline{Q}_{45}^{(k)}(\frac{\partial \phi_i}{\partial x}\frac{\partial \phi_j}{\partial y} + \frac{\partial \phi_i}{\partial y}\frac{\partial \phi_j}{\partial x}))\mathrm{d}x\mathrm{d}y)
\end{aligned}
\tag{10.1}
$$

$$
\begin{aligned}
B_{ij} &= -k_s h_c \int_{\Omega_e} G_{xz}\frac{\partial \phi_i}{\partial x}\phi_j \,\mathrm{d}x\mathrm{d}y \\[6pt]
&-k_s\sum_{k=1}^{L}(z_k - z_{k-1})(\int_{\Omega_e}(\overline{Q}_{44}^{(k)}\frac{\partial \phi_i}{\partial x} + \overline{Q}_{45}^{(k)}\frac{\partial \phi_i}{\partial y})\phi_j \,\mathrm{d}x\mathrm{d}y
\end{aligned}
\tag{10.2}
$$

$$C_{ij} = -k_s h_c \int_{\Omega_e} G_{yz} \frac{\partial \phi_i}{\partial y} \phi_j \, \mathrm{d}x\mathrm{d}y$$
$$-k_s \sum_{k=1}^{L} (z_k - z_{k-1})(\int_{\Omega_e} (\bar{Q}_{45}^{(k)}\frac{\partial \phi_i}{\partial x} + \bar{Q}_{55}^{(k)}\frac{\partial \phi_i}{\partial y})\phi_j \, \mathrm{d}x\mathrm{d}y$$

(10.3)

$$D_{ij} = \frac{1}{6}\sum_{k=1}^{L}(z_k^3 - z_{k-1}^3)(\int_{\Omega_e} (\bar{Q}_{11}^{(k)}\frac{\partial \phi_i}{\partial x}\frac{\partial \phi_j}{\partial x} + \bar{Q}_{66}^{(k)}\frac{\partial \phi_i}{\partial y}\frac{\partial \phi_j}{\partial y}$$
$$+\bar{Q}_{16}^{(k)}(\frac{\partial \phi_i}{\partial x}\frac{\partial \phi_j}{\partial y} + \frac{\partial \phi_i}{\partial y}\frac{\partial \phi_j}{\partial x}))\mathrm{d}x\mathrm{d}y) + \frac{1}{2}k_s(\sum_{k=1}^{L}\bar{Q}_{44}^{(k)}(z_k - z_{k-1}) + h_c G_{xz})\int_{\Omega_e} \phi_i \phi_j \, \mathrm{d}x\mathrm{d}y$$

(10.4)

$$F_{ij} = \frac{1}{6}\sum_{k=1}^{L}(z_k^3 - z_{k-1}^3)(\int_{\Omega_e} (\bar{Q}_{22}^{(k)}\frac{\partial \phi_i}{\partial y}\frac{\partial \phi_j}{\partial y} + \bar{Q}_{66}^{(k)}\frac{\partial \phi_i}{\partial x}\frac{\partial \phi_j}{\partial x}$$
$$+\bar{Q}_{26}^{(k)}(\frac{\partial \phi_i}{\partial y}\frac{\partial \phi_j}{\partial x} + \frac{\partial \phi_i}{\partial x}\frac{\partial \phi_j}{\partial y}))\mathrm{d}x\mathrm{d}y) + \frac{1}{2}k_s(\sum_{k=1}^{L}\bar{Q}_{55}^{(k)}(z_k - z_{k-1}) + h_c G_{yz})\int_{\Omega_e} \phi_i \phi_j \, \mathrm{d}x\mathrm{d}y$$

(10.5)

$$H_{ij} = \frac{1}{6}\sum_{k=1}^{L}(z_k^3 - z_{k-1}^3)(\int_{\Omega_e} (\bar{Q}_{12}^{(k)}\frac{\partial \phi_i}{\partial x}\frac{\partial \phi_j}{\partial y} + \bar{Q}_{16}^{(k)}\frac{\partial \phi_i}{\partial x}\frac{\partial \phi_j}{\partial x} + \bar{Q}_{26}^{(k)}\frac{\partial \phi_i}{\partial y}\frac{\partial \phi_j}{\partial y}$$
$$+\bar{Q}_{66}^{(k)}\frac{\partial \phi_i}{\partial y}\frac{\partial \phi_j}{\partial x})\mathrm{d}x\mathrm{d}y) + \frac{1}{2}k_s(\sum_{k=1}^{L}\bar{Q}_{45}^{(k)}(z_k - z_{k-1}))\int_{\Omega_e} \phi_i \phi_j \, \mathrm{d}x\mathrm{d}y$$

(10.6)

$$i, j = 1,2,3\ldots 16$$

A convenient measure of structural damping is the specific damping capacity, SDC, usually shown by the symbol Ψ (not to be confused with the plate rotations shown in Fig. 2), which is defined as the ratio of the damping energy to the maximum strain energy, thus

$$\Psi = \frac{\Delta U}{U}$$

(11)

Similar to the strain energy, we assume that the damping energy of the sandwich element is also a piecewise function of the damping energies of the skins and the core, thus

$$\Delta U_e = \frac{1}{2}\sum_{k=1}^{L}\int_{z_{k-1}}^{z_k}(\int_{\Omega_e}\{\varepsilon\}^T[R_s^{(k)}]\{\varepsilon\}\,\mathrm{d}x\mathrm{d}y)\mathrm{d}z + \frac{1}{2}\int_{-\frac{h_c}{2}}^{\frac{h_c}{2}}(\int_{\Omega_e}\{\varepsilon\}^T[R_c]\{\varepsilon\}\,\mathrm{d}x\mathrm{d}y)\mathrm{d}z$$

(12)

in which the skin damped stiffness matrix $[R_s^{(k)}]$ and core damped stiffness matrix $[R_c]$ are given in terms of the damping matrixes $[\Psi_s]$ and $[\Psi_c]$ as

$$[R_s] = [T]_\sigma^{-1}[\Psi_s][Q][T]_\varepsilon \tag{13.1}$$

$$[R_c] = [\Psi_c][G_c] \tag{13.2}$$

where the damping matrixes $[\Psi_s]$ and $[\Psi_c]$ are the diagonal matrixes

$$[\Psi_s] = \begin{bmatrix} \Psi_{11} & 0 & 0 & 0 & 0 \\ 0 & \Psi_{22} & 0 & 0 & 0 \\ 0 & 0 & \Psi_{13} & 0 & 0 \\ 0 & 0 & 0 & \Psi_{23} & 0 \\ 0 & 0 & 0 & 0 & \Psi_{12} \end{bmatrix} \tag{14.1}$$

$$[\Psi_c] = \begin{bmatrix} 0 & 0 & 0 & 0 & 0 \\ 0 & 0 & 0 & 0 & 0 \\ 0 & 0 & \Psi_{xz} & 0 & 0 \\ 0 & 0 & 0 & \Psi_{yz} & 0 \\ 0 & 0 & 0 & 0 & 0 \end{bmatrix} \tag{14.2}$$

in which the factors $[\Psi_{ij}]$ quantify the proportion of the energy loss in each cycle of vibration due to the relevant stress components.

It is noted that the skin and core stiffness Equations (3) and the analogous damping equations (14) reflect the assumption that while the in-plane damping of the honeycomb material can be neglected with little loss of accuracy, the shear damping of the skins can be significant depending on the skin/core relative thickness.

From equation (9), the element damping energy is accordingly given as

$$\Delta U_e = \overline{A}_{ij} w_i w_j + \overline{B}_{ij} w_i \psi_{xj} + \overline{C}_{ij} w_i \psi_{yj} + \overline{D}_{ij} \psi_{xi} \psi_{xj} + \overline{F}_{ij} \psi_{yi} \psi_{yj} + \overline{H}_{ij} \psi_{xi} \psi_{yj} \tag{15}$$

in which

$$\overline{A}_{ij} = \frac{1}{2} k_s h_c \int_{\Omega_e} \left(\Psi_{xz} G_{xz} \frac{\partial \phi_i}{\partial x} \frac{\partial \phi_j}{\partial x} + \Psi_{yz} G_{yz} \frac{\partial \phi_i}{\partial y} \frac{\partial \phi_j}{\partial y} \right) dxdy + \frac{1}{2} k_s \sum_{k=1}^{L} (z_k - z_{k-1})$$

$$\left(\int_{\Omega_e} \left(R_{44}^{(k)} \frac{\partial \phi_i}{\partial x} \frac{\partial \phi_j}{\partial x} + R_{55}^{(k)} \frac{\partial \phi_i}{\partial y} \frac{\partial \phi_j}{\partial y} + R_{45}^{(k)} \left(\frac{\partial \phi_i}{\partial x} \frac{\partial \phi_j}{\partial y} + \frac{\partial \phi_i}{\partial y} \frac{\partial \phi_j}{\partial x} \right) \right) dxdy \right) \tag{16.1}$$

$$\overline{B}_{ij} = -k_s h_c \int_{\Omega_e} \Psi_{xz} G_{xz} \frac{\partial \phi_i}{\partial x} \phi_j \, dxdy$$
$$-k_s \sum_{k=1}^{L} (z_k - z_{k-1})(\int_{\Omega_e} (R_{44}^{(k)} \frac{\partial \phi_i}{\partial x} + R_{45}^{(k)} \frac{\partial \phi_i}{\partial y}) \phi_j \, dxdy)$$

(16.2)

$$\overline{C}_{ij} = -k_s h_c \int_{\Omega_e} \Psi_{yz} G_{yz} \frac{\partial \phi_i}{\partial y} \phi_j \, dxdy$$
$$-k_s \sum_{k=1}^{L} (z_k - z_{k-1})(\int_{\Omega_e} (R_{45}^{(k)} \frac{\partial \phi_i}{\partial x} + R_{55}^{(k)} \frac{\partial \phi_i}{\partial y}) \phi_j \, dxdy)$$

(16.3)

$$\overline{D}_{ij} = \frac{1}{6} \sum_{k=1}^{L} (z_k^3 - z_{k-1}^3)(\int_{\Omega_e} (R_{11}^{(k)} \frac{\partial \phi_i}{\partial x} \frac{\partial \phi_j}{\partial x} + R_{66}^{(k)} \frac{\partial \phi_i}{\partial y} \frac{\partial \phi_j}{\partial y}$$
$$+R_{16}^{(k)}(\frac{\partial \phi_i}{\partial x} \frac{\partial \phi_j}{\partial y} + \frac{\partial \phi_i}{\partial y} \frac{\partial \phi_j}{\partial x}))dxdy) + \frac{1}{2} k_s (\sum_{k=1}^{L} R_{44}^{(k)}(z_k - z_{k-1}) + h_c \Psi_{xz} G_{xz}) \int_{\Omega_e} \phi_i \phi_j \, dxdy$$

(16.4)

$$\overline{F}_{ij} = \frac{1}{6} \sum_{k=1}^{L} (z_k^3 - z_{k-1}^3)(\int_{\Omega_e} (R_{22}^{(k)} \frac{\partial \phi_i}{\partial y} \frac{\partial \phi_j}{\partial y} + R_{66}^{(k)} \frac{\partial \phi_i}{\partial x} \frac{\partial \phi_j}{\partial x}$$
$$+R_{26}^{(k)}(\frac{\partial \phi_i}{\partial y} \frac{\partial \phi_j}{\partial x} + \frac{\partial \phi_i}{\partial x} \frac{\partial \phi_j}{\partial y}))dxdy) + \frac{1}{2} k_s (\sum_{k=1}^{L} R_{55}^{(k)}(z_k - z_{k-1}) + h_c \Psi_{yz} G_{yz}) \int_{\Omega_e} \phi_i \phi_j \, dxdy$$

(16.5)

$$\overline{H}_{ij} = \frac{1}{6} \sum_{k=1}^{L} (z_k^3 - z_{k-1}^3)(\int_{\Omega_e} (R_{12}^{(k)} \frac{\partial \phi_i}{\partial x} \frac{\partial \phi_j}{\partial y} + R_{16}^{(k)} \frac{\partial \phi_i}{\partial x} \frac{\partial \phi_j}{\partial x} + R_{26}^{(k)} \frac{\partial \phi_i}{\partial y} \frac{\partial \phi_j}{\partial y}$$
$$+R_{66}^{(k)} \frac{\partial \phi_i}{\partial y} \frac{\partial \phi_j}{\partial x})dxdy) + \frac{1}{2} k_s (\sum_{k=1}^{L} R_{45}^{(k)}(z_k - z_{k-1})) \int_{\Omega_e} \phi_i \phi_j \, dxdy$$
$$i, j = 1, 2, 3 \dots 16$$

(16.6)

The element's kinetic energy is given as

$$T_e = \frac{1}{2} \omega^2 \int_{\Omega_e} (2\rho_s(h - h_c)w^2 + \frac{1}{12}(\rho_s(h^3 - h_c^3) + \rho_c h_c^3)(\psi_x^2 + \psi_y^2)) dxdy$$

(17)

in which ω is the natural frequency, h is the total panel thickness, and ρ_s and ρ_c are skin and core mass densities respectively. Substituting for w, ψ_x and ψ_y from equation (7) in equation (17) will give the latter equation as

$$T_e = \omega^2 (m_{ij} w_i w_j + I_{ij}(\psi_{xi}\psi_{xj} + \psi_{yi}\psi_{yj}))$$

(18)

in which

$$m_{ij} = \rho_s(h - h_c)\int_{\Omega_e} \phi_i\phi_j \, \mathrm{d}x\mathrm{d}y$$

$$I_{ij} = \frac{1}{24}(\rho_s(h^3 - h_c^3) + \rho_c h_c^3)\int_{\Omega_e} \phi_i\phi_j \, \mathrm{d}x\mathrm{d}y \qquad , \quad i,j = 1,2,3\ldots16 \tag{19}$$

The displacements within each element of the discretised plate are computed from the displacements in the sixteen nodes that immediately surround the element (Figure 3) using the lagrangian quadrilateral interpolating functions. Hence, the displacement functions in each element 1 are computed from the nodes that are shared by that element and the three successive neighboring elements on each side. The sixteen nodes that surround the element are effectively the support domain that is used in the meshless method. This support domain has an overlap with the surrounding elements which should ensure the continuity of the displacements and their first and second derivatives at the elements' boundaries.
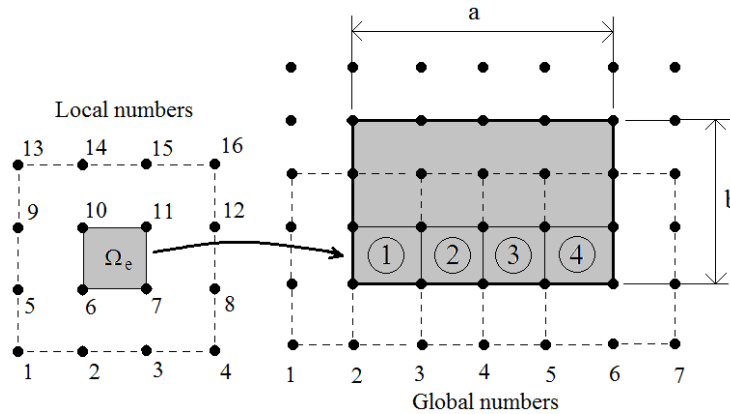
Figure 3: Elements and their shared domains in a rectangular plate.

The total strain, damping and kinetic energies of the plate in terms of the elemental energies are given respectively as

$$U = \sum_{e=1}^{n} U_e, \ \Delta U = \sum_{e=1}^{n}\Delta U_e, \ T = \sum_{e=1}^{n}T_e \tag{20}$$

in which n is the number of elements. Since the total energy of the system is constant at any given time, one may write

$$U - T = \text{constant}, \tag{21}$$

thus,

$$\left\{ \begin{array}{c} \left\{ \dfrac{\partial(U-T)}{\partial w_i} \right\} \\[2em] \left\{ \dfrac{\partial(U-T)}{\partial \psi_{xi}} \right\} \\[2em] \left\{ \dfrac{\partial(U-T)}{\partial \psi_{yi}} \right\} \end{array} \right\} = 0 \ , \quad i = 1, 2, 3 \ldots N \tag{22}$$

in which N is the total number of nodes. One may further write

$$\left\{ \begin{array}{c} \left\{ \dfrac{\partial U}{\partial w_i} \right\} \\[1.5em] \left\{ \dfrac{\partial U}{\partial \psi_{xi}} \right\} \\[1.5em] \left\{ \dfrac{\partial U}{\partial \psi_{yi}} \right\} \end{array} \right\} = [K] \left\{ \begin{array}{c} \{w_i\} \\ \{\psi_{xi}\} \\ \{\psi_{yi}\} \end{array} \right\}, \quad \left\{ \begin{array}{c} \left\{ \dfrac{\partial T}{\partial w_i} \right\} \\[1.5em] \left\{ \dfrac{\partial T}{\partial \psi_{xi}} \right\} \\[1.5em] \left\{ \dfrac{\partial T}{\partial \psi_{yi}} \right\} \end{array} \right\} = \omega^2 [M] \left\{ \begin{array}{c} \{w_i\} \\ \{\psi_{xi}\} \\ \{\psi_{yi}\} \end{array} \right\} \ , \quad i = 1, 2, 3 \ldots N \tag{23}$$

in which $[K]$ and $[M]$ are the stiffness and mass matrices respectively. In order to determine the elements of the stiffness and mass matrices of the panel, the elemental stiffness and mass matrices are considered

$$\left\{ \begin{array}{c} \left\{ \dfrac{\partial U_e}{\partial w_i} \right\} \\[1.5em] \left\{ \dfrac{\partial U_e}{\partial \psi_{xi}} \right\} \\[1.5em] \left\{ \dfrac{\partial U_e}{\partial \psi_{yi}} \right\} \end{array} \right\} = [K_e] \left\{ \begin{array}{c} \{w_i\} \\ \{\psi_{xi}\} \\ \{\psi_{yi}\} \end{array} \right\} \ , \quad i = 1, 2, 3 \ldots 16 \tag{24}$$

$$\left\{ \begin{array}{c} \left\{ \dfrac{\partial T_e}{\partial w_i} \right\} \\[1.5em] \left\{ \dfrac{\partial T_e}{\partial \psi_{xi}} \right\} \\[1.5em] \left\{ \dfrac{\partial T_e}{\partial \psi_{yi}} \right\} \end{array} \right\} = \omega^2 [M_e] \left\{ \begin{array}{c} \{w_i\} \\ \{\psi_{xi}\} \\ \{\psi_{yi}\} \end{array} \right\} \ , \quad i = 1, 2, 3 \ldots 16 \tag{25}$$

Using Equation (9) in equation (24), the elemental stiffness matrix is given as

$$[K_e] = \begin{bmatrix} [A^*] & [B] & [C] \\ & [D^*] & [H] \\ Sym & & [F^*] \end{bmatrix} \tag{26}$$

in which

$$\begin{aligned} A^*_{ij} &= A_{ij} + A_{ji} \\ D^*_{ij} &= D_{ij} + D_{ji} \quad , \quad i,j = 1,2,3\ldots16 \\ F^*_{ij} &= F_{ij} + F_{ji} \end{aligned} \tag{27}$$

where A_{ij}, B_{ij} etc. have been given in Equations (10).

Similarly, the elemental mass matrix is given by Equations (18) and (25) as

$$[M_e] = \begin{bmatrix} [M^*] & 0 & 0 \\ & [I^*] & 0 \\ Sym & & [I^*] \end{bmatrix} \tag{28}$$

in which

$$\begin{aligned} M^*_{ij} &= m_{ij} + m_{ji} \\ I^*_{ij} &= I_{ij} + I_{ji} \end{aligned} \quad , \quad i,j = 1,2,3\ldots16 \tag{29}$$

where m_{ij} and I_{ij} have been given in Equations (19).

As shown in Figure 3, the nodes are denoted by both the local as well as global numbers. The element matrices $[K_e]$ and $[M_e]$ are obtained using the local numbers, and the elements of these matrices are lodged in the global matrices $[K]$ and $[M]$ using the interrelationship between the local and the global numbers, thus obtaining the full global matrices. By substituting these matrices in Equations (23) before substituting the resulting equations into Equation (22), the following generalized eigenvalue problem is obtained, the solution of which yields the natural frequencies and mode shapes of the panel

$$\left([K] - \omega^2 [M]\right) \begin{Bmatrix} \{w_i\} \\ \{\psi_{xi}\} \\ \{\psi_{yi}\} \end{Bmatrix} = 0 \quad , \quad i = 1,2,3\ldots N \tag{30}$$

The eigenvector produces nodal displacements that have been assigned a global number. Again, the interrelation between the local and the global nodal numbers is used to determine the local nodal displacements, and hence the strain and damping energies, of each element. The SDC for each mode is then computed by using the first two of the energy equations (20) in equation (11).

The method of solution in this study can be generalized for a panel with any arbitrary shape, as well as a rectangular geometry. In Figure 4, one such arbitrary shape is considered. The nature of the node distribution shown is what is typically required for the analysis, in that the extension of node distribution beyond the boundary is needed to provide the support domain for the boundary elements.
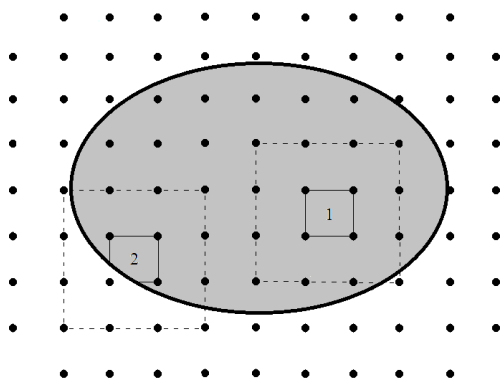
Figure 4: Defining the geometry of the problem.

As the figure indicates, for an arbitrary geometry two types of elements are used. The type 1 element lies entirely within the panel and, therefore, is the same element as previously introduced in Figure 1. However, the type 2 element shown in Figure 5, lies on the plate boundary and is no longer of a rectangular shape. In order to compute the stiffness and mass matrices of this element, it is only necessary to carry out the integrals in Equations (10) and (19) within the geometric bounds of this element.
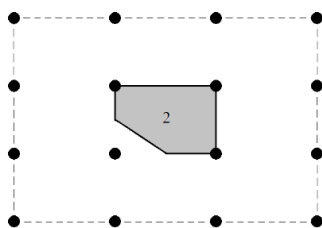
Figure 5: The type 2 element.

Thus, the procedure for the solution of the problem outlined in Figure 4 is the same as that for a rectangular plate except that the integrations are carried out to within the actual boundary of the type 2 element.

It is possible to extend the analysis in an analogous manner to include the through-thickness dimension as well, thereby removing the need for the requirement of an explicit formulation for the lateral shear deformations. However, the solution would obviously expend a substantially more computational resources than a two-dimensional analysis.

3   RESULTS

The sandwich panels considered are made from CFRP skins and aluminium or Nomex honeycomb core materials. The mechanical and damping properties of the skins and of the core are given in the following tables. It is noted that these data are actual test results which have been obtained in previous works for the CFRP skin (Maheri et al., 2008) and the honeycomb core (Adams and Maheri, 1993). The honeycomb web is aligned along the x direction (Figure 2).

E_1 (GPa)	E_2 (GPa)	G_{12} (GPa)	Ψ_1 (%)	Ψ_2 (%)	Ψ_{12} (%)	Ψ_{13} (%)	Ψ_{23} (%)	v_{12}	ρ (kg/m3)
271.0	6.02	5.46	0.45	7.30	8.16	8.16	8.16	0.34	1563.3

Table 1: [-60, 0, 60] CFRP skin mechanical and damping data.

G_{xz} (MPa)	G_{yz} (MPa)	Ψ_{xz} (%)	Ψ_{yz} (%)	ρ (kg/m3)
140.0	75.4	0.74	1.02	40.39

Table 2: Aluminium core honeycomb mechanical and damping data.

G_{xz} (MPa)	G_{yz} (MPa)	Ψ_{xz} (%)	Ψ_{yz} (%)	ρ (kg/m3)
40.0	29.0	11.2	10.5	40.43

Table 3: Nomex core honeycomb mechanical and damping data.

Modal response results were obtained for a number of mid-plane symmetric, carbon fibre reinforced polymer (CFRP) skin, honeycomb core sandwich panels with arbitrary geometries and different boundary conditions. Direct comparison with published results were possible only in the case of rectangular plates with all-free boundary conditions (Table 4), since these were the only compatible published results available.

Table 4 shows a comparison of the present results with those of (Maheri et al., 2008) where the method of Rayleigh-Ritz (RR) as well as experimental measurements (Exp) have been used to produce modal data for the all-free, rectangular panels with CFRP skins and aluminium honeycomb core. A high degree of correlation is observed between the present results and both the theoretical and the experimental results of the earlier work. It should be pointed out, however, that the test results quoted in Table 4 have been obtained for testing the plate *in-vacuo*, as the proportion of air-damping is significantly high in the overall damping of light sandwich structures (Maheri et al., 2008).
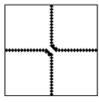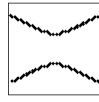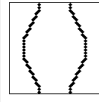
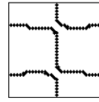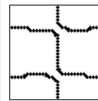| CFRP skin, Alum. HC core panels: a=b= 400 (mm), h_c = 24.315 (mm), h = 24.915 (mm)					
Mode Shape					
Freq. (Hz)	Present method	795	1225	1474	1814
	Numeric (Maheri et al., 2008)	796	1221	1469	1817
	Experiment (Maheri et al., 2008)	757	1202	1471	1755
SDC. (%)	Present method	1.06	1.03	0.78	0.99
	Numeric (Maheri et al., 2008)	1.03	1.00	0.76	0.97
	Experiment (Maheri et al., 2008)	1.11	1.51	1.06	1.21

Table 4: Comparison of the present results with those of (Maheriet al.,2008)
for a symmetric, CFRP skin, aluminium HC core sandwich panel

In Table 5, the results of a mesh-refinement examination have been tabulated for the first four modes of the above plate. These results show that while convergence of the SDC results in all modes occurs for as coarse as a 6×6 nodes mesh, a somewhat finer 10×10 mesh would suffice to ensure of a complete convergence in both the frequency and damping values in all the modes considered. The present results were obtained using a 14×14 mesh.
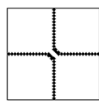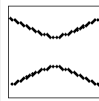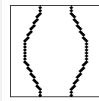
CFRP skin, Alum. HC core panels: a=b= 400 (mm), h_c = 24.315 (mm), h = 24.915 (mm)								
Quantity of nodes	Freq. (Hz)	SDC. (%)	Freq. (Hz)	SDC. (%)	Freq. (Hz)	SDC. (%)	Freq. (Hz)	SDC. (%)
4×4	803.9	1.05	1358.7	1.06	1719.3	0.74	2090.9	0.98
6×6	798.5	1.06	1251.6	1.04	1522.8	0.77	1861.4	0.98
8×8	796.1	1.06	1227.9	1.03	1479.0	0.78	1818.9	0.99
10×10	795.6	1.06	1225.9	1.03	1475.3	0.78	1815.1	0.99
12×12	795.5	1.06	1225.6	1.03	1474.8	0.78	1814.4	0.99
14×14	795.4	1.06	1225.4	1.03	1474.3	0.78	1814.2	0.99
16×16	795.4	1.06	1225.4	1.03	1474.3	0.78	1814.2	0.99

Table 5: An examination of the mesh refinement requirement for complete convergence.

Tabulated in Tables 6, to 9 are the modal characteristics, including modal damping, of symmetric sandwich panels with different geometries. In each case, free (F) and/or clamped (C) edges have been considered.
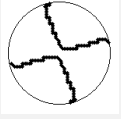
CFRP skin, Nomex. HC core panels: a=b= 400 (mm), h_c=24.315, h= 24.915 (mm)				
Mode Shape (CCCC)				
Freq. (Hz)	814.1	1239.0	1347.6	1665.1
SDC. (%)	9.7745	9.8721	10.0962	10.2235
Mode Shape (CCCF)				
Freq. (Hz)	583.7	968.8	1094.5	1400.8
SDC. (%)	9.0122	8.8828	9.5757	9.7142
Mode Shape (CCFF)				
Freq. (Hz)	306.0	721.3	800.3	1154.7
SDC. (%)	6.1249	8.0177	8.3659	9.0493
Mode Shape (CFCF)				
Freq. (Hz)	605.0	713.6	1150.4	1211.0
SDC. (%)	9.6462	8.8021	8.7383	9.9814
Mode Shape (CFFF)				
Freq. (Hz)	196.1	355.4	725.4	936.9
SDC. (%)	4.4649	6.2149	8.0913	8.3440
Mode Shape (FFFF)				
Freq. (Hz)	595.9	889.5	1012.8	1125.4
SDC. (%)	5.9674	6.7851	7.1415	8.2916

Table 6: Modal characteristics results for the symmetric, CFRP skin, Nomex.
HC core sandwich panels with different boundary conditions.
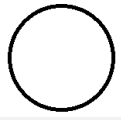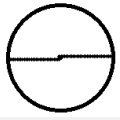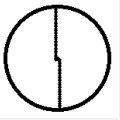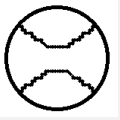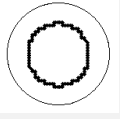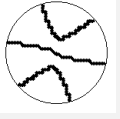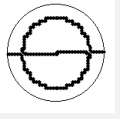
CFRP skin, Nomex. HC core panels: d= 400 (mm), h$_c$,= 24.315, h = 24.915 (mm)			
Mode Shape Clamped edge				
Freq. (Hz)	601.7	949.9	961.3	1299.0
SDC. (%)	9.9240	9.7237	9.5659	9.5414
Mode Shape Free edge				
Freq. (Hz)	896.1	1285.4	1422.9	1424.7
SDC. (%)	6.8606	8.1703	8.8596	8.8468

Table 7: Modal characteristics results for the symmetric, CFRP skin,
Nomex. HC core circular panels with free and clamped edges.
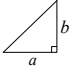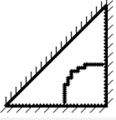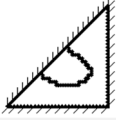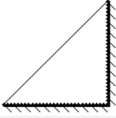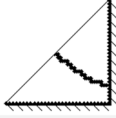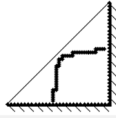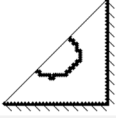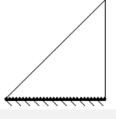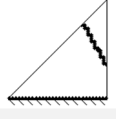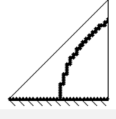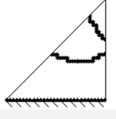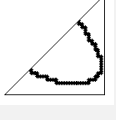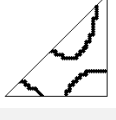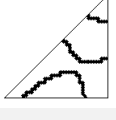
CFRP skin, Nomex. HC core panels: a=b= 400 (mm), h$_c$,= 24.315, h= 24.915 (mm)			
Mode Shape CCC				
Freq. (Hz)	1348.7	1902.1	2185.1	2488.3
SDC. (%)	10.4005	10.4153	10.4806	10.5082
Mode Shape CCF				
Freq. (Hz)	787.9	1268.7	1615.5	1820.5
SDC. (%)	9.1864	9.6788	9.6950	9.9518
Mode Shape CFF				
Freq. (Hz)	292.8	733.6	901.3	1291.1
SDC. (%)	5.9824	7.9784	7.4185	9.0745
Mode Shape FFF				
Freq. (Hz)	837.2	1116.7	1407.5	1420.5
SDC. (%)	6.6980	7.6200	8.7411	8.5280

Table 8: Modal characteristics results for the symmetric, CFRP skin,
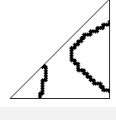Nomex. HC core triangular panels with different boundary conditions.

CFRP skin, Nomex. HC core panels:
a=b= 400 (mm), h_c =24.315, h= 24.915 (mm)
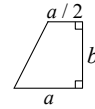
Mode Shape CCCC				
Freq. (Hz)	1030.3	1419.7	1751.8	1882.7
SDC. (%)	10.1838	10.1574	10.3458	10.2493
Mode Shape CCCF				
Freq. (Hz)	624.3	1088.5	1261.7	1577.5
SDC. (%)	8.7628	9.4860	9.1760	9.8772
Mode Shape CCFF				
Freq. (Hz)	510.7	844.6	1238.1	1340.2
SDC. (%)	7.9008	8.7065	9.1239	9.3688
Mode Shape CFFF				
Freq. (Hz)	211.9	511.2	676.7	1056.4
SDC. (%)	5.2095	6.5687	7.9930	8.4498
Mode Shape FFFF				
Freq. (Hz)	721.5	906.0	1169.1	1271.3
SDC. (%)	6.4716	7.1738	8.0930	8.2458

Table 9: Modal characteristics results for the symmetric, CFRP skin,
Nomex. HC core Trapezoid panels with different boundary conditions.

The results in these tables show that a correlation generally exists between the amount of the fixity of the plate and the modal damping, in that damping increases with the number of fixed edges. Restricted edges inhibit the movement of the skins relative to each other and this increases the degree of the interlocking between the lateral displacement of the plate and the shear deformation of the core, resulting in increased core damping. Furthermore, increased fixity of the panel makes modal damping increasingly invariant of the sandwich mode shape.

4 CONCLUSIONS

Modal damping of sandwich panels comprising FRP skins and a honeycomb core can be computed using the mixed finite element-meshless technique. This is a viable and accurate method for predicting the modal response of sandwich panels with arbitrary geometries and different boundary conditions. The method is versatile, in that it can readily and conveniently use the same initially set-up node and element distributions to analyse different geometries. Furthermore, the continuity of the displacements at the elements' boundaries are assured.

A number of sandwich panels with different geometries and boundary conditions were considered and, where possible, the modal characteristics, including the damping results were compared with those reported in the literature, whereupon it was shown that a high degree of correlation exists between the two sets of results. It was further shown that as the number of fixed edges increases, the sandwich damping increases and it becomes increasingly invariant of the sandwich mode shape.

References

Adams, R.D., Maheri, M.R., (1993). The dynamic shear properties of structural honeycomb materials. Composites Science and Technology 47: 15-23.

Elmalich, D., Rabinovitch, O., (2012). A high-order finite element for dynamic analysis of soft-core sandwich plates. Journal of Sandwich Structure and Materials 14(5): 525–555.

Koo, K.N., Lee, I., (1995). A refined analysis of vibration and damping for anisotropic laminates in cylindrical bending. Journal of Sound and Vibration 184(4): 553-566.

Liu, Q., Zhao, Y., (2001). Prediction of Natural Frequencies of a Sandwich Panel Using Thick Plate Theory. Journal of Sandwich Structure and Materials 3: 289-309.

Liu, Q., Zhao, Y., (2007). Effect of Soft Honeycomb Core on Flexural Vibration of Sandwich Panel using Low Order and High Order Shear Deformation Models. Journal of Sandwich Structure and Materials 9: 95-108.

Maheri, M.R., Adams, R.D., (1994). Steady-state flexural vibration damping of honeycomb sandwich beams. Composites Science and Technology 52: 333-347.

Maheri, M.R., Adams, R.D., Hugon, J., (2008). Vibration damping in sandwich panels. Journal of Materials Science 43: 6604-6618.

Meunier, M., Shenoi, R.A., (2001). Dynamic analysis of composite sandwich plates with damping modelled using high-order shear deformation theory. Composite Structures 54: 243-254.

Phan, C., Frostig, Y., Kardomateas, G.A., (2013). Free vibration of unidirectional sandwich panels, Part II: Incompressible core. Journal of Sandwich Structure and Materials 15(4): 412–428.

Soovere, J., (1984). Dynamic Response of Acoustically Excited Stiffened Composite Honeycomb Panels. PhD Thesis, ISVR: University of Southampton.

Thamburaj, P., Sun, J.Q., (2001). Effect of Material and Geometry on the Sound and Vibration Transmission across a Sandwich Beam. Journal of Vibration and Acoustics 123: 205-212.

Yaman, M., Onal, T., (2015). Investigation of dynamic properties of natural material-based sandwich composites: Experimental test and numerical simulation. Journal of Sandwich Structure and Materials 0(00): 1–18.

Yim, J.H., Gillespie, J.W., (2000). Damping characteristics of 0° and 90° AS4/3501-6 unidirectional laminates including the transverse shear effect. Composite Structures 50: 217-225.

Zhao, D., Stronge, W.J., (2006). Modal Frequencies of Circular Sandwich Panels. Journal of Sandwich Structure and Materials 8: 343-357.